

RSC Advances



This is an *Accepted Manuscript*, which has been through the Royal Society of Chemistry peer review process and has been accepted for publication.

Accepted Manuscripts are published online shortly after acceptance, before technical editing, formatting and proof reading. Using this free service, authors can make their results available to the community, in citable form, before we publish the edited article. This *Accepted Manuscript* will be replaced by the edited, formatted and paginated article as soon as this is available.

You can find more information about *Accepted Manuscripts* in the [Information for Authors](#).

Please note that technical editing may introduce minor changes to the text and/or graphics, which may alter content. The journal's standard [Terms & Conditions](#) and the [Ethical guidelines](#) still apply. In no event shall the Royal Society of Chemistry be held responsible for any errors or omissions in this *Accepted Manuscript* or any consequences arising from the use of any information it contains.

Bottom-Up Nanoarchitectonics of Two-Dimensional Freestanding Metal Doped Carbon Nanosheet

Hicham Hamoudi^{1,2*}

International Center for Young Scientists (ICYS)¹

*International Center for Materials Nanoarchitectonics (WPI- MANA), National Institute for
Materials Science (NIMS)², 1-1 Namiki, Tsukuba, 305-0044, Japan*

Abstract

Through appropriate engineering of the 5,5'-Bis(mercaptomethyl)-2,2'-bipyridine self-assembled monolayer (BPD-SAM) on a gold surface, ultrathin sulfur functionalized freestanding carbon-metal nanosheets (CMNS) have been produced. The BPD-SAM was used to encapsulate Ni⁺². The resulting BPD-Ni⁺² SAM was cross-linked by high-energy electrons. The nanomembrane was realized by dissolving the gold substrate. The chemical and physical properties of the CMNS were investigated using X-ray photoelectron spectroscopy (XPS), UV-vis reflection spectroscopy, atomic force microscopy (AFM), scanning electron microscopy (SEM), energy dispersive X-ray (EDX), and electrical two-point probe measurements.

Keywords: self-assembled monolayers, carbon-metal nanosheet, crosslinking

Author information

Corresponding authors: H. Hamoudi: Phone: +81-29-851-3354 (ext.8672), FAX: +81-29-860-4706, E-mail: Hamoudi.hicham@nims.go.jp

Introduction

As early as 1930, Langmuir and Blodgett assembled molecules on a water surface to form membranes known as Langmuir–Blodgett films.¹ Molecular monolayer self-assembly is an experimental approach to form highly ordered monolayers on various substrates.^{2, 3, 4} Self-assembled monolayers (SAMs) show similarities to the biological membranes, where the lipids self-organize via intramolecular interaction. SAMs containing aromatic groups show a high degree of order. They can be useful as building blocks to create new hybrid materials with novel functionalities out of the scope of traditional solid-state devices.^{5, 6, 7, 8} It has been shown recently that modification of the aromatic SAMs on different solid surfaces by electron beams enables fabrication of carbon nanomembranes (CNM) through crosslinking of the aromatic SAM.^{9, 13} Low-energy electron beams are necessary to create the crosslinked molecular network. Exposure of the conjugate SAMs to high-energy electron beams enables the fabrication of sheets of nanometer size, which also provides evidence that the aromatic self-assembled monolayer acts as a negative electron resist for high-energy electron beams.⁹ These carbon nanofilms are separable from their substrates and are transferred onto new holders.¹⁰ The CNM can be biofunctionalized with anchoring molecules, which enable their use for widely various biological applications. Moreover, CNM annealing has a strong impact on the electrical and electronic properties of these materials.¹¹

Engineering the band gap of the 2D materials such as graphene by metal doping is an important challenge confronting scientists. In the literature, no attempt has been made to dope carbon nanosheets with metals. Engineering the carbon nanosheets by adsorbates such as transition metal can modify the ground state and the magnetic properties of the nanosheets. A redox-active center such as (Ni) has been incorporated into the organic backbones to improve the charge-transfer processes. Different studies of molecular redox center immobilized on metallic substrate indicate them as good conductors.²⁹ This report describes a simple method to build a new material regarded as sulfur functionalized freestanding carbon–metal nanosheet (CMNS), based on a crosslinked self-assembled monolayer SAM of (5,5'-Bis(mercaptomethyl)-2,2'-bipyridine)-Ni⁺² (BPD-Ni) as shown in Figure 1. The BPD SAM was crosslinking by high-energy electron irradiation. Dissolving the Au underlying substrate releases the CMNS.

The membrane was characterized by various complementary techniques such as X-ray photoelectron spectroscopy, UV-vis reflection spectroscopy, atomic force microscopy, scanning electron microscopy, energy dispersive X-ray (EDX), and electrical two-point probe measurements.

The dithiols molecules provide an active interface to the nanosheet, and can be tailored to adsorb a various materials, such as metals. In biological applications this nanosheet can be used as biocompatible interfaces for surface immobilization of, e.g., cells and proteins.

Experimental section

5,5'-Bis (mercaptomethyl)-2,2'-bipyridine was purchased from Aldrich and used as received. The gold substrates were prepared by thermal evaporation of 150 nm of gold (99.99% purity) onto either polished single-crystal silicon (100) wafers primed with a 10 nm titanium adhesion layer or on freshly cleaved mica at 340 °C. The SAM of the 5,5'-bismercaptomethyl-2,2'-bipyridine (BPD) (Figure 1) was prepared by immersing the gold support into a freshly prepared 1 mM solution of n-hexane for 1 h at about 60 °C. Solutions that had been well-degassed by Ar, and all preparation steps were performed in the absence of ambient light, following the same protocol as in our previous studies.¹⁴ Subsequently, the gold wafer, modified with a layer of BPD, was held for 3 h in contact with a concentrated aqueous solution of NiCl₂.

XPS spectroscopy measurements were conducted at the MANA Foundry using an XPS spectrometer (XPS version Alpha 110 mm Analyser; Thermo Fisher). The XPS spectra were recorded in the Au 4f, S 2p, C 1s, N 1s, and Ni 2p regions. The spectra acquisition was performed in normal emission geometry using Al K α radiation. The binding energy (BE) scale of each spectrum was calibrated individually to the Au 4f_{7/2} emission at 83.95 eV.

The AFM topographical and phase images were collected using a SPM microscope (diMultimode; Veeco Instruments) in tapping mode. To measure the film thickness, the freely suspended membranes were placed on the silicon wafer. Its edge area was scanned. The morphology of the membranes was investigated with a scanning electron microscope (S-4300; Hitachi Ltd.) equipped with a W tip cold-FE

electron emitter. The 3×3 mm square patterns were created using an electron beam lithography system (50 kV, 70 mC/cm^2 ; Elionix Inc.). The morphology and the energy dispersive X-ray (EDX) analysis of CMNS were conducted at MANA using a transmission electron microscope (TEM, JEM-2100F; JEOL). The UV/Vis transmission mode was measured using a UV/Vis/NIR spectrophotometer (V-570; Jasco Corp.)

Results and discussion

S 2p XPS spectra of the BPD SAMs are presented in Figure 2c. The fits of the S 2p BPD SAM (Figure 2c) was performed setting a 1.2 eV $2p_{1/2, 3/2}$ splitting and introducing two doublets: The first doublet was at 162 eV S_1 commonly assigned to the thiolate species, this BE value corresponds to the thiolate species bonded to Au metal surfaces. The second doublet at about ~ 163.7 eV S_2 corresponding to sulfur of the free thiol (SH) groups or S–S bonds.^{14, 15, 16, 17, 18, 19}

The N 1s XPS spectra of the BPD SAM are presented in Figure 2b. A single symmetric peak at 399 eV is assigned to the nitrogen in the pyridine rings. The BPD film thickness calculated from the carbon to Au XPS signal ratio using the dodecanethiol (DDT) SAM as reference is ~ 2 nm, which shows good agreement with the BPD molecule height.

The C 1s spectra of the BPD film and the reference dodecanthiol (DDT) SAM are displayed in Figure 2a. The main peak at 285.5 eV is a superposition of the contribution from different carbons: the aliphatic moieties (CH_2) and the meta, para C in the pyridine unit, and the ortho C in the rings bound directly to the nitrogen atoms.²⁰

Treatment of the BPD SAM with NiCl_2 (Figure 1) brings a significant change to the S 2p and the N 1s spectra. The S 2p spectra (Figure 2c) show a clear change in the relative intensity of both components S_1 and S_2 after exposure to Ni, which is probably attributable to the partial formation of the Ni thiolate species at the SAM–ambient interface.^{21, 22} Indeed, the intensity of the free S (S_2 peak) at the SAM

interface decreases in intensity with respect to the Au (/metal) bound S (S1 peak), indicating partial linkage to Ni.²⁶ In addition, it is noteworthy that the dithiols SAMs are extremely sensitive to photo-oxidation [4, 6]. Solutions that are well-degassed by Ar and the absence of ambient light during the preparation steps can minimize oxidation. The peak at 168 eV was assigned to the partial formation of the sulfonate at the interface, which was probably produced during the cleaning and transfer of the samples. It should be noted that they have no Cl contaminant in the SAM.

In the case of N 1s spectra (Figure 2b), The addition of Ni produces a splitting of the main peak, the first moiety (unaffected by Ni) at the same energy as N1s of the BPD SAM, the second component towards a higher binding energy by 1.2 eV, which is a fingerprint of the binding of the bipyridine to the Ni⁺² moiety. 27, 28

Figure 2d shows the Ni 2 p_{3/2} region. The peak at 856.6 eV is assigned to Ni⁺². A diagram of the final SAM is shown in Figure 1.

The exposure of the BPD-Ni SAM to electron beams engenders the formation of a crosslinked SAM, as described earlier. In Figure 3a, the BPD-Ni/Au template was patterned using electrons (50 kV, 70 mC/cm²) and using a metal mesh as a mask. The patterned template was etched in an I₂/KI-etch bath and rinsed with *N,N*-dimethylformamide DMF. As Figure 3b shows, the optical microscope image shows that the underlying gold substrate within the irradiation areas was unaffected by the etching process. Figure 4a shows similar behavior for the BPD-Ni/Au-mica template after patterning and I₂/KI-etch treatment. This constitutes evidence that the crosslinked mechanism took place in the BPD-Ni SAM after radiation because the crosslinked SAM is more resistant to etching, although it was etched within the non-irradiated region.

Figure 4b displays sheets of BPD-Ni/Au that were released from gold after I₂/KI-etch and DMF ultrasonic treatment. This release occurs by the scission of the anchor group-substrate bonds using I₂/KI and rinsing with *N,N*-dimethylformamide DMF.¹³ Small flakes of the nanomembrane are also visible in Figure 4a.

The CMNS are released by dissolution of the underlying substrate according to well-established protocols described in an earlier report.¹⁰ In brief, a 300-nm-thick PMMA was spin-coated onto a 3 × 3 mm square of the crosslinked film and baked at 180 °C for 3 min on a hotplate. The gold film was cleaved from the mica in hydrofluoric acid solution and etched away in an I₂/KI bath. In the next step, the

nanomembrane/PMMA was transferred onto a SiO₂ substrate followed by dissolution of the PMMA in acetone to release a CMNS.

The morphologies of the fabricated nanosheet were initially investigated using scanning electron microscopy (SEM) and atomic force microscopy (AFM). Figure 5 shows AFM and SEM images of the CMNS that has been transferred from gold onto a silicon wafer (Figures 5a and 5c) and a TEM grid (Figure 5d). The SEM image shows that the CMNS was flat, and folded at the edges. The nanosheet thickness determined by AFM (Figure 5b) was about 2.9 nm for the BPD-Ni nanomembrane, which shows good agreement with the thickness obtained using XPS for the related SAM.

The chemical composition of the freestanding nanomembrane has been investigated using XPS, energy dispersive X-ray (EDX), and UV-vis spectroscopies. Figure 6 shows the C 1s, N 1s, S 2p, and Ni 2p spectra of the CMNS deposited on SiO₂ substrates. The S 2p XPS spectra of the BPD-Ni nanomembrane are shown in Figure 6c. The high background in the S2p spectrum hinder the analysis of the spectra, which is due to the influence of the Si (2s) peak located at region between 150 and 155 eV. The spectra of the former films exhibit two distinct features. The main broad and distinctly asymmetric peak at <164 eV for the BPD-Ni systems is a superposition of the contributions from the Ni-thiolate species and the disulfide (S–S) linkages or free thiol groups, whereas the second located at <168.00 eV is associated with the sulfur atom bonded to the oxygen. The C 1s XPS spectrum shows some amount of COOH in the membrane probably due to the etching process. No remarkable changes in the N 1s, and Ni 2p XPS spectra were compared to the BPD-Ni SAM before the irradiation. To investigate this further, elemental mapping of C, S, N, and Ni using energy dispersive X-ray (EDX) analysis (Figure 7) was undertaken. The result shows a homogeneous distribution of S, N, and Ni on the nanosheet. In addition, it should be noted that 38 wt% of S and 11 wt% of Ni, were detected in the composite. This result, coupled with the XPS result, provides evidence for the presence of Ni on the nanosheet. However by analyzing the Ni/N XPS single ratio of both CMNS and the BPD-Ni SAM, the nanomembrane lose around 18% of Ni after the crosslinking and itching procedure. An important shortcoming is that the sheets are often damaged during peeling and transfer to other supports.

Figure 8 shows The UV-vis measurement of the CMNS compared to the PBD without Ni incorporation. The BPD shows a band at ~ 292 nm, the CNMS in the transmission mode shows characteristic metal-to-ligand charge-transfer (MLCT) bands in the region between 300 and 370 nm. These bands are attributed to intraligand $\pi \rightarrow \pi^*$ transition. The splitting in bands of BPD-Ni (312.91 and 341.7 nm) is characteristic for the formation of Ni^{+2} -5,5'-Bis (mercaptomethyl)-2,2'-bipyridine complex.^{23,24}

The CMNS were electrically tested on a probe station using a semiconductor parameter analyzer (Keithley Instruments Inc.) using two-probe measurement at room temperature and under vacuum to avoid the influence of water. Typical I - V characteristic of the CMNS are shown in Figure 9. Each curve corresponds to a measurement in different areas on the CMNS. The I - V curve of the contact made directly on top of the CMNS exhibits a molecular behavior. At low bias, the current increases linearly with applied bias. However, at high bias the current increases exponentially with applied voltage, which is expected for a metal-alkanedithiol-metal junction.²⁵ According to the I - V result, I suggest that the electron-induced crosslinking generates mostly a σ bond between the molecules.

Conclusions

In summary, this report describes a novel method of fabricating a carbon nanosheet with encapsulated metal that involves modification of a (5,5'-Bis (mercaptomethyl)-2,2'-bipyridine) SAM using high-energy electrons. The author fabricated a freestanding organometallic nanomembrane with 3 nm thickness and a large lateral dimension. After crosslinking of the (BPD- Ni^{+2}) SAMs, the CMNS were released by dissolving the underlying substrate or by scission of the anchor group-substrate bonds. Using a combination of several complementary experimental techniques, the chemical properties of the nanomembrane were investigated: the XPS, EDX and UV-

vis analyses revealed the presence of the Ni^{+2} in the CMNS backbone. The complexation of the bipyridine functionality by Ni^{+2} is supported by the splitting of the intraligand $\pi \rightarrow \pi^*$ transition bands in the UV-vis spectra and by the shift in the N 1s XPS spectra.

The fabricated CMNS displays interesting semiconducting behavior that can be useful for molecular electronics applications. Further studies are in progress in our institute to elucidate the electron transfer mechanism in junctions based on a CMNS. The CMNS was functionalized using sulfur to accommodate further architectures such as the growth of biological systems, and grafting of different metallic structures.

Acknowledgments

I appreciate the help of Pr. Kohei Uosaki and the valuable assistance of MANA foundry. This work has been supported by the International Center for Young Scientists (ICYS) on Materials Nanoarchitectonics (WPI –MANA).

References

1. Blodgett, K. B. *USA Patent* **1940**, 2220860.
2. Nuzzo, R. G.; Fusco, F. A.; Allara, D. L. Spontaneously organized molecular assemblies. Preparation and properties of solution adsorbed monolayers of organic disulfides on gold surfaces. *J. Am. Chem. Soc.* **1987**, *109*, 2358–2368.
3. Ulman, A. An Introduction to Ultrathin Organic Films: Langmuir -Blodgett to Self-Assembly; Academic Press: New York, 1991. *A. Chem. Rev.* **1996**, *96*, 1533–1554.
4. Schreiber, F. Self-assembled monolayers: from ‘simple’ model systems to biofunctionalized interfaces. *J. Phys: Condens. Matter* **2004**, *16*, R881–R900.
5. Reed, M. A.; Zhou, C.; Muller, C. J.; Burgin, T. P.; Tour, J. M. Conductance of a molecular junction. *Science* **1997**, *278*, 252–254.
6. Baunach, T.; Ivanova, V.; Kolb, D. M.; Boyen, H. G.; Ziemann, P.; Buttner, M.; Oelhafen, P. A New Approach to the Electrochemical Metallization of Organic Monolayers: Palladium Deposition onto a 4,4'-Dithiodipyridine Self-Assembled Monolayer. *Adv. Mater.* **2004**, *16*, 2024–2028.
7. Rocha, A. R. *et al.* Towards molecular spintronics. *Nature Mater.* **2005**, *4*, 335–339.
8. Hamoudi, H.; Nepl, S.; Kao, P.; Schüpbach, B.; Feulner, P.; Terfort, A.; Allara, D.; Zharnikov, M. Orbital-Dependent Charge Transfer Dynamics in Conjugated Self-Assembled Monolayers. *Phys. Rev. Lett.* **2011**, *107*, 027801.
9. Lercel, M. J.; Craighead, H. G.; Parikh, A. N.; Seshadri, K.; Allara, D. L. Sub-10 nm lithography with self-assembled monolayers. *Appl. Phys. Lett.* **1996**, *68*, 1504.
10. Turchanin, A.; Beyer, A.; Nottbohm, C.; Zhang, X.; Stosch, R.; Sologubenko, A.; Mayer, J.; Hinze, P.; Weimann, T.; Golzhauser, A. One Nanometer Thin Carbon Nanosheets with Tunable Conductivity and Stiffness. *Adv. Mat.* **2009**, *21*, 1233–1237.
11. Turchanin, A.; Golzhauser, A. Carbon nanomembranes from self-assembled

monolayers: Functional surfaces without bulk. *Pro. Sur. Sci.* **2012**, *87*, 108–162.

12. Olsen, C.; Rowntree, P. A. Bond-selective dissociation of alkanethiol based self-assembled monolayers adsorbed on gold substrates, using low-energy electron beams. *J. Chem. Phys.* **1997**, *108*, 3750–3763.

13. Eck, W.; Kuller, A.; Grunze, M.; Volkel, B.; Golzhauser, A. Freestanding Nanosheets from Crosslinked Biphenyl Self-Assembled Monolayers. *Adv. Mater.* **2005**, *17*, 2583–2587.

14. Hamoudi, H.; Prato, M.; Dablemont, C.; Canepa, M.; Esaulov, V. A. Self-Assembly of 1,4-Benzenedimethanethiol Self-Assembled Monolayers on Gold. *Langmuir* **2010**, *26*, 7242–7247.

15. Hamoudi, H.; Guo, Z. A.; Prato, M.; Dablemont, C.; Zheng, W. Q.; Bourguignon, B.; Canepa, M.; Esaulov, V. A. On the self-assembly of short chain alkanedithiols. *Phys. Chem. Chem. Phys.* **2008**, *10*, 6836–6841.

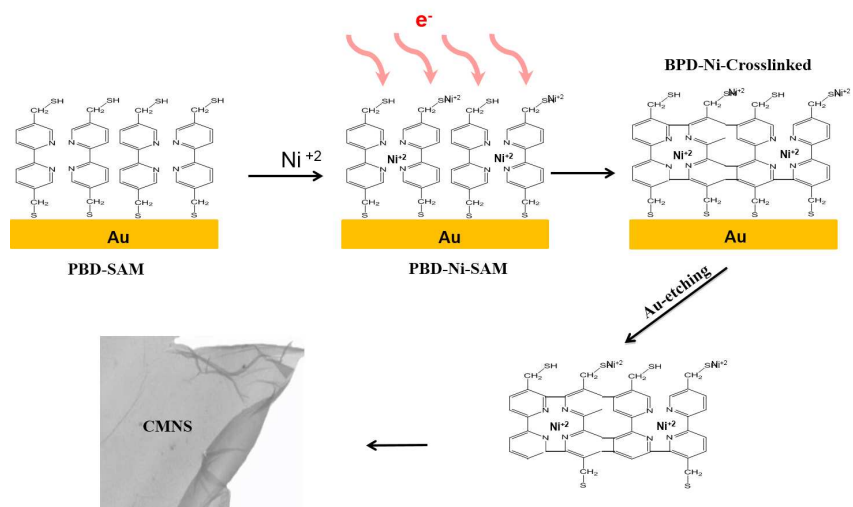
16. Pasquali, L.; Terzi, F.; Zanardi, C.; Pigani, L.; Seeber, R.; Paolicelli, G.; Suterin, S. M.; Mahne, N.; Nannarone, S. Structure and properties of 1,4-benzenedimethanethiol films grown from solution on Au (111): An XPS and NEXAFS study. *Surf. Sci.* **2007**, *601*, 1419–1427.

17. Pasquali, L.; Terzi, F.; Seeber, R.; Doyle, B. P.; Nannarone, S. Adsorption geometry variation of 1,4-benzenedimethanethiol self-assembled monolayers on Au (111) grown from the vapor phase. *J. Chem. Phys.* **2008**, *128*, 134711.

18. Pasquali, L.; Terzi, F.; Seeber, R.; Nannarone, S.; Datta, D.; Dablemont, C.; Hamoudi, H.; Canepa, M.; Esaulov, V. A. UPS, XPS, and NEXAFS Study of Self-Assembly of Standing 1,4-Benzenedimethanethiol SAMs on Gold. *Langmuir* **2011**, *27*, 4713–4720.

19. Nakanishi, T.; Ohtani, B.; Uosaki, K. Fabrication and characterization of CdS nanoparticle mono- and multilayers on a self-assembled monolayer of alkanedithiols on gold. *J. Phys. Chem. B* **1998**, *102*, 1571–1577.
20. Hamoudi, H.; Döring, K.; Chesneau, F.; Lang, H.; Zharnikov, M. Self-Assembly of Pyridine-Substituted Alkanethiols on Gold: The Electronic Structure Puzzle in the Ortho- and Para-Attachment of Pyridine to the Molecular Chain. *J. Phys. Chem. C* **2012**, *116*, 861–870.
21. Esplandiu, M. J.; Noeske, P. L. M. XPS investigations on the interactions of 1,6-hexanedithiol/Au (111) layers with metallic and ionic silver species. *Appl. Surf. Sci.* **2002**, *199*, 166–182.
22. Tai, Y.; Shaporenko, A.; Eck, W.; Grunze, M.; Zharnikov, M. Abrupt change in the structure of self-assembled monolayers upon metal evaporation *Appl. Phys. Lett.* **2004**, *85*, 6257.
23. Gilliam, A. E.; Hey, D. H.; Lambert, A. The absorption spectra of the phenylpyridines and pyridyldiphenyls. *J. Chem. Soc.* **1941**, 364–367.
24. Pilz, C. S.; Steinem, C. Modulation of the conductance of a 2,2'-bipyridine-functionalized peptidic ion channel by Ni²⁺. *Eur. Biophys. J.* **2008**, *37*, 1065–1071.
25. Hylke, B.; Akkerman, P.; Blom W. M.; de Leeuw Bert de Boer, D. M. Towards molecular electronics with large-area molecular junctions. *Nature* **2006**, *441*, 69–72.
26. Tortech, L.; Mekhalif, Z.; Delhalle, J.; Guittard, F.; Geribaldi, S. Self-assembled monolayers of semifluorinated thiols on electrochemically modified polycrystalline nickel surfaces. *Thin Solid Films* **2005**, *491*, 253–259.
27. Liu G, Klein A, Thissen A, Jaegermann W: Electronic properties and interface characterization of phthalocyanine and Ru-polypyridine dyes on TiO₂ surface. *Surf. Sci.* **2003**, *539*, 37–48.

28. Agnes C, Arnault J-C, Omnes F, Bruno J, Billon M, Bidand G, Mailley P: XPS study of ruthenium tris-bipyridine electrografted from diazonium salt derivative on microcrystalline boron doped diamond. *Phys. Chem. Chem. Phys.* **2009**, *11*, 11647–11654.29.
29. Tuccitto N, Ferri V, Cavazzini M, Quici S, Zhavnerko G, Licciardello A, Rampi M A: Highly Conductive 40-nm Long Molecular Wires Assembled by Stepwise Incorporation of Metal Centres. *Nature Materials* **2009**, *8*, 41–46.



TOC image: Fabrication of freestanding carbon–metal–sulfide nanosheet from a self-assembled monolayer.

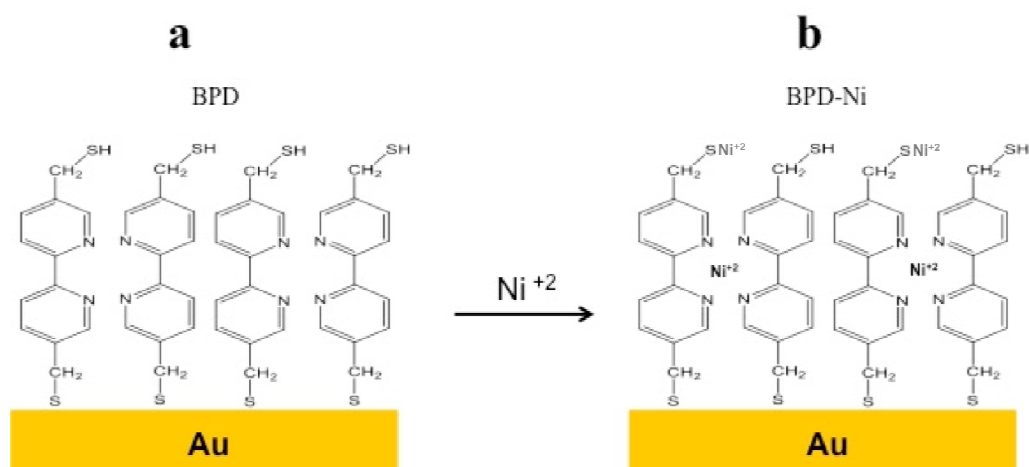


Figure 1. Scheme of sequential reactions to prepare BPD-Ni monolayer. (a) Self-assembly monolayer (SAM) of the BPD on Au (111). (b) Proposed configuration of BPD-Ni SAM after Ni encapsulation.

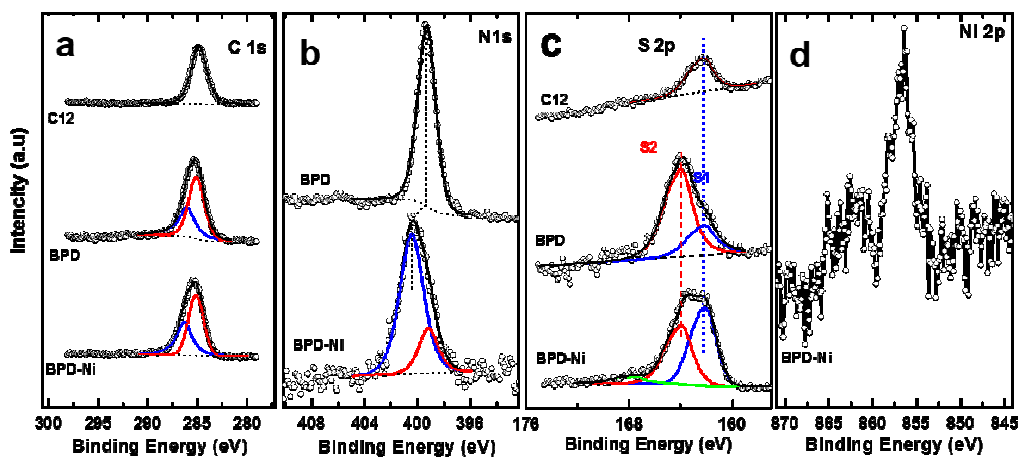


Figure 2. XPS spectra of the BPD and BPD-Ni SAMs on gold: (a) C 1s, (b) N 1s, (c) S 2p, and (d) Ni 2p. Some spectra are decomposed into the individual contributions related to different species; see the text for details.

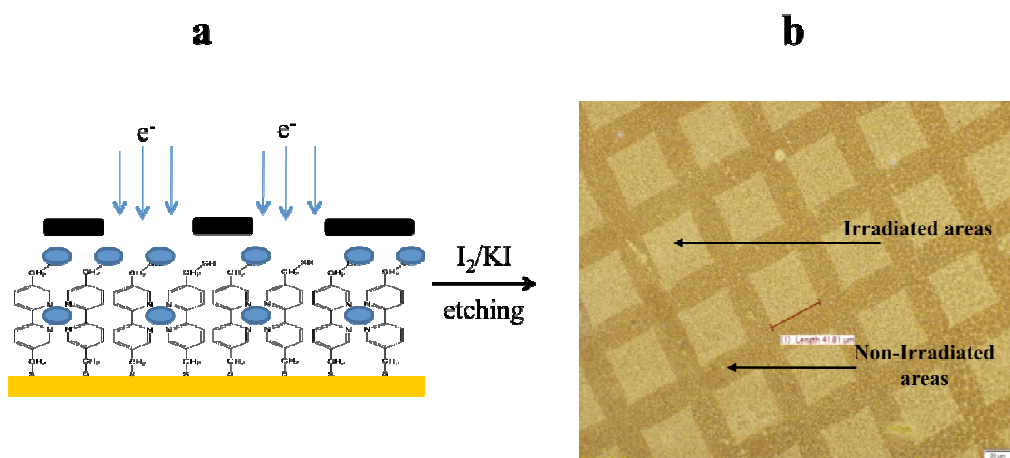


Figure 3. A BPD-Ni system was used as a negative resist for e-beam lithography. (a) Scheme demonstrating the radiation of the BPD-Ni SAM through a mask. (b) Microscopic image of etched BPD-Ni /Au template, preliminarily patterned by electrons in proximity printing geometry using a metal mesh as mask. The areas exposed and not exposed to electrons are marked.

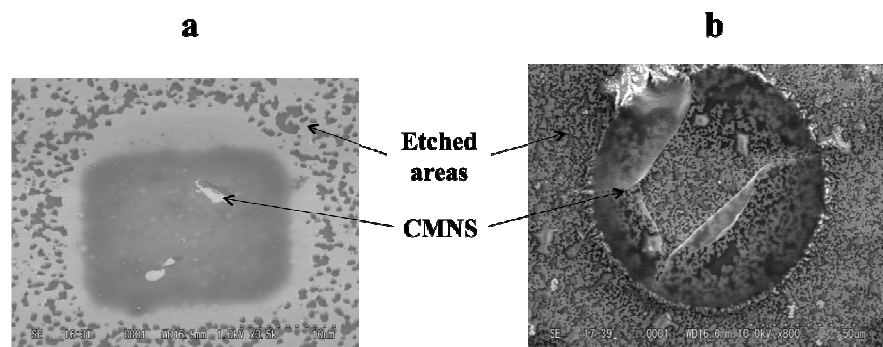


Figure 4. SEM images of Au patterns fabricated by proximity printing lithography with (a) square pattern of a monolayer of BPD-Ni and (b) BPD-Ni nanomembrane (after DMF ultrasonic treatment).

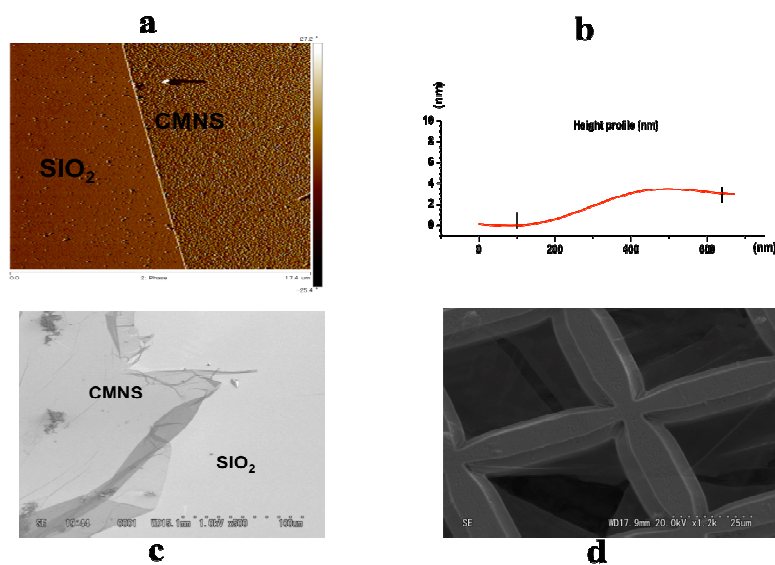


Figure 5. AFM and SEM images of CMNS. The CMNS was prepared using electron radiation of structure b (see Figure 1) and then detached by dissolving the gold substrate: (a) AFM image of the CMNS on SiO_2 ; (b) AFM height profile of the CMNS on SiO_2 ; (c) SEM image of the CMNS deposited on a SiO_2 substrate; (d) SEM image of the CMNS deposited on a TEM grid.

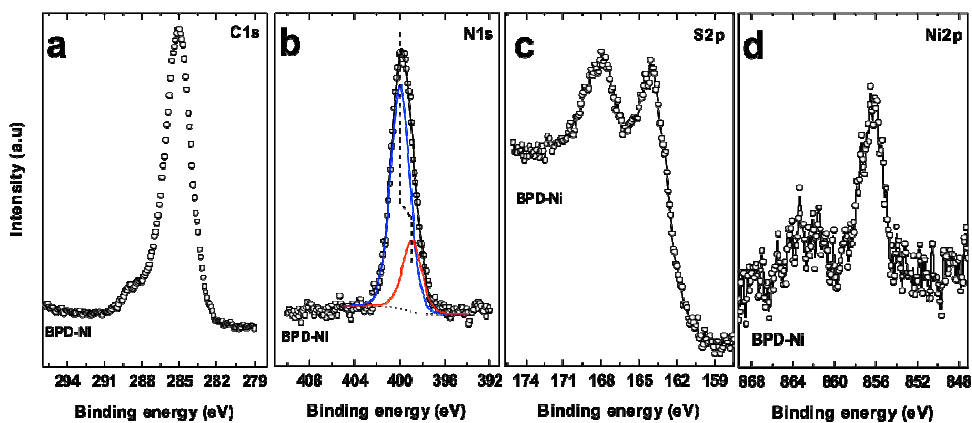


Figure 6. XPS spectra of the CMNS: (a) C 1s, (b) N 1s, (c) S 2p, and (d) Ni 2p. The N 1s spectra have decomposed into individual contributions related to the different species; see the text for details.

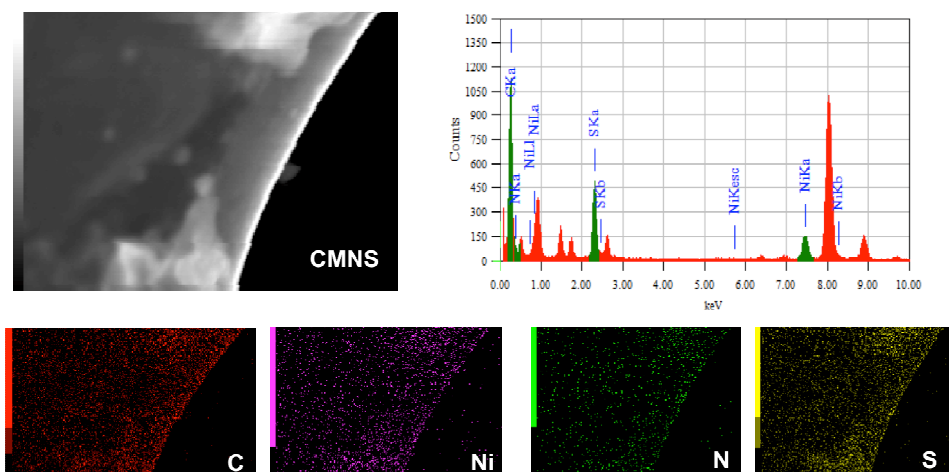


Figure 7. Typical transmission electron microscopy (TEM) image, EDX spectrum of the CMNS, and corresponding elemental mapping images of C, N, Ni, and S show the homogeneous dispersion of Ni in the CMNS.

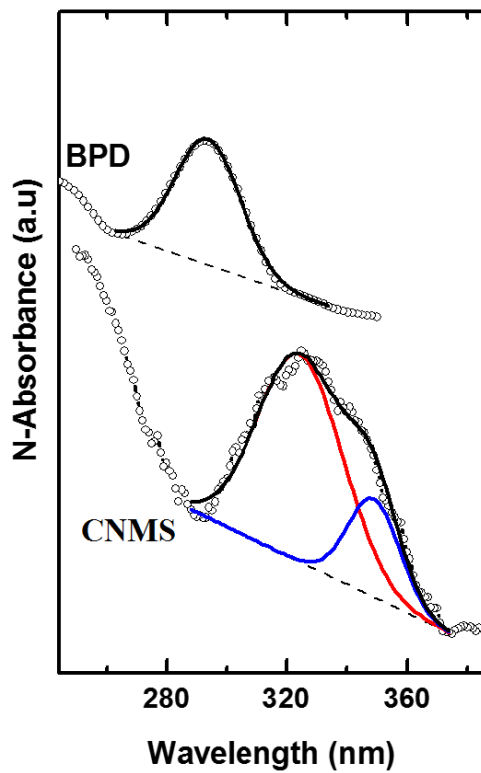


Figure 8. UV-vis spectra of the BPD and the CMNS deposited on a SiO₂.

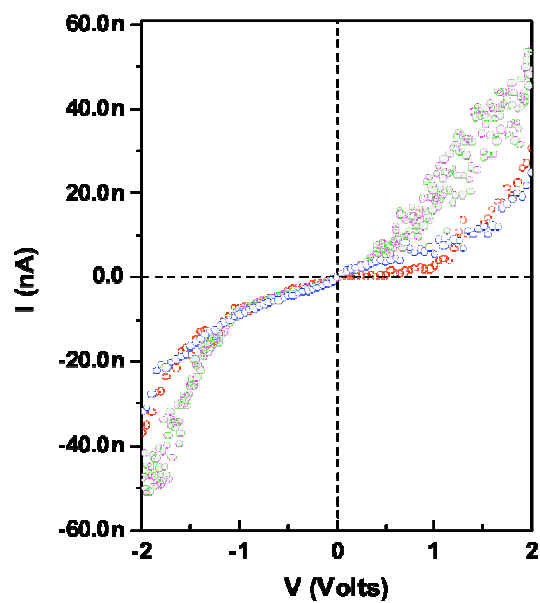


Figure 9. Room-temperature current versus voltage of the CMNS. Each curve corresponds to a measurement in a different area on top of CMNS.